ROYAL SOCIETY OF CHEMISTRY

CrystEngComm

Hydrothermally stable transition alumina by condensation-enhanced self-assembly and pyrolysis crystallization. Application in the steam reforming of methane.

SCHOLARONE™
Manuscripts

Journal Name

CrystEngComm

Dynamic Article Links ▶

ARTICLE TYPE

Hydrothermally stable transition alumina by condensation-enhanced self-assembly and pyrolysis crystallization. Application in the steam reforming of methane.

Lidia López Pérez,[a] Consuelo Alvarez-Galván,[b] Valeriya Zarubina,[a] Bruno O. Figueiredo Fernandes[a]
5 and Ignacio Melián-Cabrera[a]*

The preparation of a steam-based hydrothermally stable transition alumina is reported. The gel is derived from a synthetic sol-gel route where Al-tri-*sec*-butoxide is hydrolysed in the presence of a non-ionic
10 surfactant ($EO_{20}PO_{70}EO_{20}$), HCl as catalyst and water ($H_2O/Al=6$); the condensation is strengthened by treating the hydrolysed gel with tetrabutyl ammonium hydroxide (TBAOH) and it is dried afterwards at 60°C by solvent evaporation. The so-obtained mesophase is crystallized under Argon at 1200°C (1 h) giving rise to a transitional alumina containing δ/α, and possibly θ, alumina. Due to the surface acidity, the pyrolysis conditions transform the block copolymer into a cross-linked char that embeds the alumina
15 crystallites. Calcination at 650°C fully generates the porosity by burning the char; a residual carbon of 0.2 *wt*.% was found, attributed to the formation of surface (oxy)carbides. As a result, this route produces a transition alumina formed by nanoparticles of about 30 nm on average, surface areas ranging 59-76 $m^2\,g^{-1}$ with well-defined mesopores centered at 14 nm. The material withstands steam at 900°C with a relative surface area rate loss lower than δ-aluminas, state-of-the art MSU-X γ-alumina and those reported for
20 other pure γ-aluminas. The hydrothermal stability is confirmed under relevant CH_4 steam reforming conditions, after adding Ni; a much lower surface area decay and higher CH_4 conversion was found when compared to a state-of-the-art MSU-X based Ni-catalyst. Two effects are important to explain the properties of such an alumina; the char protects the particles against sintering, however, the dominant effect is provided by the TBAOH treatment that makes the mesophase more resistant to coarsening and
25 sintering.

Introduction

In heterogeneous catalysis and separation processes (*a.o.* adsorption, chromatography) transition aluminas are by far the most used inorganic material. Industrially, alumina precursors are
30 generally produced by four routes; flask calcination, aluminate acidi-fication, neutralization of Al salts and alkoxide hydrolysis.[1] Typical precursors are gibbsite, bayerite, boehmite (pseudo-boehmite, crystalline and highly crystallized) and diaspore; the latter is normally produced from gibbsite, bayerite or boehmite at
35 pressures larger than 140 atm in the presence of steam. These precursors are thermally dehydrated into various crystalline forms

a. University of Groningen, Institute of Technology & Management, Chemical Reaction Engineering, Nijenborgh 4, 9747 AG Groningen, The Netherlands. Fax: +31 50 363 4759; Tel: +31 50 363 4267; E-mail: i.v.melian.cabrera@rug.nl
b. Sustainable Energy and Chemistry Group, Institute of Catalysis and Petroleum Chemistry, CSIC. C/ Marie Curie 2, Madrid 28049, Spain.

that depend on the applied temperature and starting precursors.[2] Thermally activated alumina phases comprise: ρ (150-250 °C); η (250–500 °C), χ (300–500 °C), γ (300–850 °C), δ (600–1000 °
40 C), κ (800–1150 °C), θ (850–1150 °C) and finally the thermo-dynamically stable α phase (>1150 °C), with the exception of the diaspore route where α-alumina can crystallize from 500 °C. These temperatures are strongly influenced by the presence of impurities or additives.

45 Due to the surface acidity and relatively high surface area, γ-alumina is the preferable crystalline phase as catalyst support or adsorbent; business examples can be found in catalytic reforming and hydro-processing in oil refinery.[3,4] Despite its maturity, there are still aspects for improvement. From a material stand point,
50 enhancing its surface area and overcoming the limited hydrothermal steam-based stability have been technical challenges. Regarding the first aspect, the limited interparticle space between the crystallites gives rise to relatively low surface areas. Most of the research has been focused on enhancing the
55 surface area while keeping a relatively narrow pore size distribution. Sol-gel routes have succeeded in obtaining γ-aluminas with well-defined mesopores by means of supra-

molecular surfactants in combination with sol-gel alkoxide routes.[5] Presently, organized mesoporous aluminas can be synthesized with partially[6-9] and well-crystallized γ-alumina walls.[10-25]

The hydrothermal stability has been the second aspect of attention. For high-temperature catalytic applications in the presence of steam, such as steam reforming, CH_4 combustion or exhaust gas converters, the reactivity and hydrothermal stability of the γ-alumina has been a very relevant drawback. Such reactivity leads to catalyst deactivation by loss of surface area, rehydration, formation of surface or bulky spinels and sintering of the supported metals. A well-known undesirable effect is the reduction of Rh dispersion in three-way catalyst converters by the formation of a $RhAl_2O_4$ spinel.[26] The above mentioned applications have found catalysts based on stabilized aluminas or hexaaluminates[27-29]; to less extent alternative refractory materials have been proposed as well.[30,31]

The simplest way for stabilizing a transition alumina against hydrothermal conditions is the introduction of structural promoters. This can be done either during the preparation of the support itself or by surface modifications of commercially available aluminas. Among these promoters, silica[32-41] lanthanum[42,43] and barium[44] are the most effective to withstand hydrothermal conditions; many others have been investigated as well.[44,45] The effect of these promoters has been identified: silica forms a layer firmly bonded to the alumina surface[34]; lanthanum forms aluminate microdomains[42] while barium generates a surface hexaalu-minate.[44] The result is the restriction of the metal oxide sintering with temperature and steam, with a slow rate of surface area loss. Typical surface areas rate losses for pure γ-alumina lies within 5-20 $m^2.g^{-1}.h^{-1}$ while those for stabilized aluminas range 0.1-3 $m^2.g^{-1}.h^{-1}$ at 600°C and 0.1 atm H_2O.[33]

It is clear from the above that the hydrothermal stabilization of aluminas has relied almost exclusively on the addition of a second component, as promoters or by forming a different crystalline phase. This prevents sintering at expense of modifying the surface properties of the alumina; see for instance the effect of silica on the acidity that was thoroughly studied by Daniel et al.[37]

An alternative to the use of promoters would consist of modifying the sol-gel synthesis route of the alumina mesophases itself, aiming to obtain more hydrothermally stable transitional aluminas after the thermal activation. This option, to the best of our knowledge, has not been reported.

In this paper we will report a transition alumina derived from a synthetic three-step sol-gel route, where the condensation step is improved by raising the pH, in combination with high-temperature pyrolysis that produces a carbon-embedded transition alumina. Calcination afterwards at lower temperature generates fully the porosity. The alumina so-obtained possesses well-defined and relatively narrow mesopores and can withstand steaming conditions at 900°C; the surface area rate loss is lower than those reported for pure aluminas and comparable to promoters-based counterparts. The synthesis protocol, structural and textural characteristics of this material is discussed thoroughly.

Experimental

Chemicals

Aluminum tri-*sec*-butoxide (97%), Pluronic P123 (M=5800,

$EO_{20}PO_{70}EO_{20}$) from Sigma-Aldrich; hydrochloric acid (37 *wt.%*) from Merck; *sec*-butyl alcohol (99%) from Acros Organics; tetrabutyl ammonium hydroxide (TBAOH, 1.0 M in methanol) supplied by Sigma-Aldrich were used in this study. A commercial γ-alumina was acquired from Merck and used as reference material for the high temperature treatments. A hydrotreatment γ-Al_2O_3 (S_{BET}=270 $m^2.g^{-1}$) was used as reference material for the acidity tests. MSU-X was acquired from Sigma-Aldrich.

Synthesis of the mesophase

The hydrolysis of the base mesophase (TBAOH-EISA) is carried out using a procedure reported by López-Pérez et al[46] in acidic medium (HCl) with a non-ionic surfactant (Pluronic P123, $EO_{20}PO_{70}$ EO_{20}), aluminum tri-*sec*-butoxide in *sec*-butanol at 60 °C; the amount of water was fixed to H_2O/Al=6 (mol); the gel before evaporation was condensed by increasing the pH up to 5 adding TBAOH solution. Further details can be found in López-Pérez et al[46]. For comparison, an alumina mesophase without the TBAOH treatment was studied as well, corresponding to the TAN-3*a* material after thermal activation. Table 1 summarizes the samples prepared with their stabilization and thermal activation protocol.

High temperature activation

The novelty of this work relies mostly on the thermal activation protocol. The activation was carried out in two steps: high-
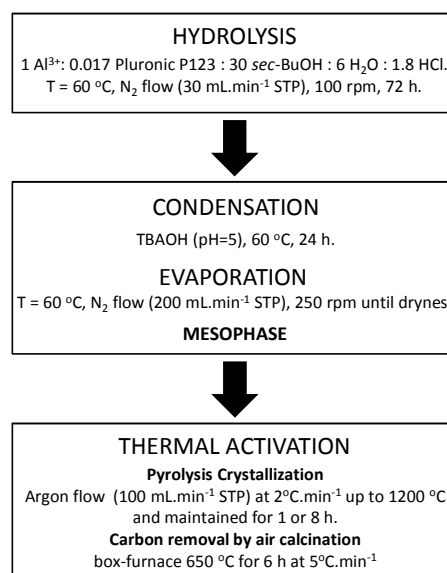

Figure 1. Synthesis protocol including sol-gel and thermal steps.

temperature pyrolysis and low-temperature calcination. In the pyrolysis step, the dried mesophase was heated in a Entech ETF 15 tube furnace using argon flow (100 mL.min^{-1} STP) at 1200 °C with a heating rate of 2 °C.min^{-1} and maintained for 1 or 8 h. The sample was placed into a 10 mL-Coors® crucible (Sigma Aldrich) that was positioned at the centre of the heating zone. These treatments produce a black hybrid material containing a char as well as the alumina phases. In the second step, the organic material is burnt by oxidation in a LT9/11 Nabertherm box furnace at 650 °C for 6 h at 5 °C.min^{-1} using static air. The calcination temperature was deduced from the TGA patterns of the intermediate pyrolyzed material, which is given in Fig. 5.

Table 1. Structural and textural data derived from N_2 adsorption at -196 °C and XRD.

Material	Stabilization	Activation	Phase [a]	S_{BET} (m^2.g^{-1}) [b]	V_T (cm^3.g^{-1})	Φ_{BJH} (nm)
TAN-1	TBAOH	1200 °C, Ar 1h	δ,θ,α	64 [c]	0.176	13.6
TAN-2	TBAOH	1200 °C, Ar 8h	α,θ	23	0.107	27, 60 [f]
TAN-3a [d]	none	1200 °C, Ar 1h	α	10	0.070	>60
TAN-4	TBAOH	1200 °C, air 1h	θ,α	39	0.140	15, 32 [f]
COM [e]	none	1200 °C, Ar 1h	α	7.5	0.018	>100

*a. Major to minor phases detected; **b.** After removing the char in air at 650 °C for 6 h; **c.** The surface area fluctuates, this corresponds to an intermediate value (see Fig. S-3); **d.** Suffix 'a' makes emphasis that this material contains pure alpha alumina; **e.** Thermally treated commercial γ-alumina (Merck); **f.** Bimodal pore size distributions having a shoulder at higher pore sizes.*

The complete sol-gel synthesis route and activation protocol are summarized in Figure 1. A control experiment (sample TAN-4) was carried out where the mesophase was calcined in air, using the same heating parameters as for TAN-1.

Steaming tests

The hydrothermal stability was evaluated by exposing the sample under 100% steam at 900 °C for 4 and 24 h. The sample was loaded in a flat quartz crucible and placed in a quartz-tube housed tubular oven (Nabertherm RT 50/250-11). The temperature was increased up to 200 °C at a heating rate of 5 °C.min^{-1}. At this temperature the sample was exposed to steam and further heated up to 900 °C (5 °C.min^{-1}) and kept for 4 and 24 h.

Characterization of the pyrolyzed materials

The burnable organic content of the pyrolyzed materials was quantified by thermogravimetric analysis (TGA) on a Mettler-Toledo analyzer (TGA/SDTA851e) using a flow of synthetic air of 100 mL.min^{-1} STP. The temperature was increased from 30 to 900 °C at 10 °C.min^{-1}. Blank curve subtraction using an empty crucible was taken into account. Powder X-ray diffraction (XRD) measurements were carried out on a Bruker D8 powder X-ray diffractometer using CuKα radiation, λ=0.154056 nm. The spectra were recorded with a step size of 0.02° for 3 s accumulation time, in the 2θ angle range of 20-80°.

Characterization of the activated materials

Nitrogen physisorption analyses at −196 °C were carried out in a Micromeritics ASAP 2420. The samples were degassed in vacuum at 350 °C for 10 h. The surface area was calculated using the standard BET method (S_{BET}, m^2.g^{-1}).[47] For surface areas below 10 m^2.g^{-1} a decimal is given. The single point pore volume (V_T, cm^3.g^{-1}) was estimated from the amount of gas adsorbed at a relative pressure of 0.98 in the desorption branch. The pore size distributions (PSD) were obtained from the BJH method[48] using the adsorption branch of the isotherms; the PSD maxima are reported as Φ_{BJH}. The t-plot method was employed to quantify the micropore volume (V_μ, cm^3.g^{-1}).[49] The particle size, d_{BET}, was calculated by using the equation $d_{BET} = 6 \cdot 10^6/(\rho \cdot S_{BET})$ where ρ is the particle skeletal density; ρ_δ=3.20·10^3 kg.m^{-3} and ρ_θ=3.56·10^3 kg.m^{-3}.[50] NH$_3$-TPD experiments were carried out in a Micromeritics Auto-Chem II following a protocol described elsewhere.[51] Elemental carbon was analysed in a EuroVector 3000 CHNS analyzer. Approximately 2 mg of sample was weighed in a 6-digit analytic balance (Mettler Toledo). The

samples were burnt at 1800 °C in the presence of an oxidation catalyst and decomposed into CO_2, H_2O, and N_2. These gases are then separated in a Porapak QS column at 80 °C and quantified with a TCD detector. Acetonitrile (99.9%) was used as an external standard. TEM and dark-field TEM (DF-TEM) images
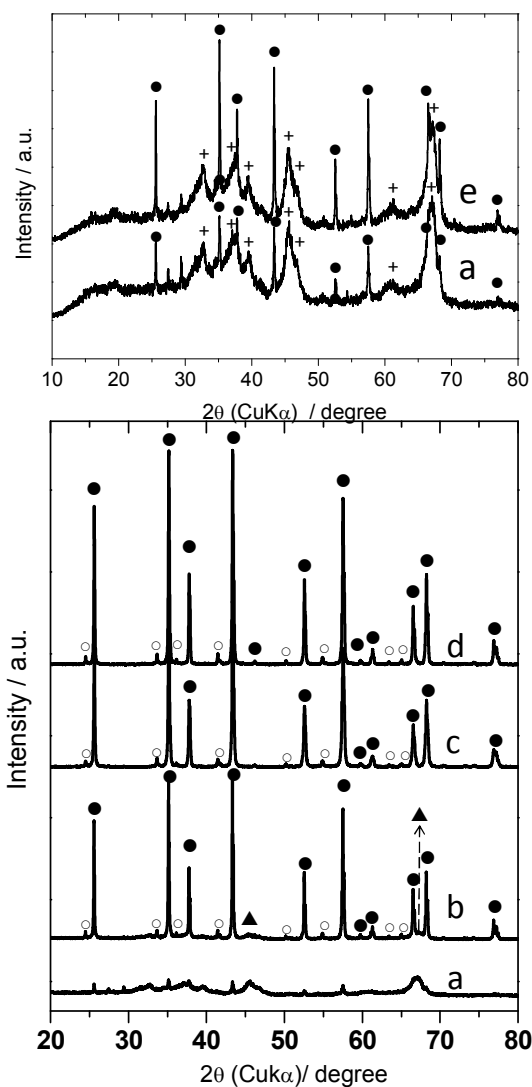

Figure 2. XRD patterns for the pyrolyzed materials at 1200 °C: **a)** TAN-l; **b)** TAN-2; **c)** TAN-3a; **d)** thermally treated commercially alumina (COM) and **e)** TAN-l after steaming at 900 °C for 24 h. Phase notation: Alpha (●)[56]; theta (▲)[57] and delta (+)[58]. Patterns **b**, **c** and **d** have a small contribution (○) that is an artefact (W-aberration)[46]. The patterns are offset in Y-axis.
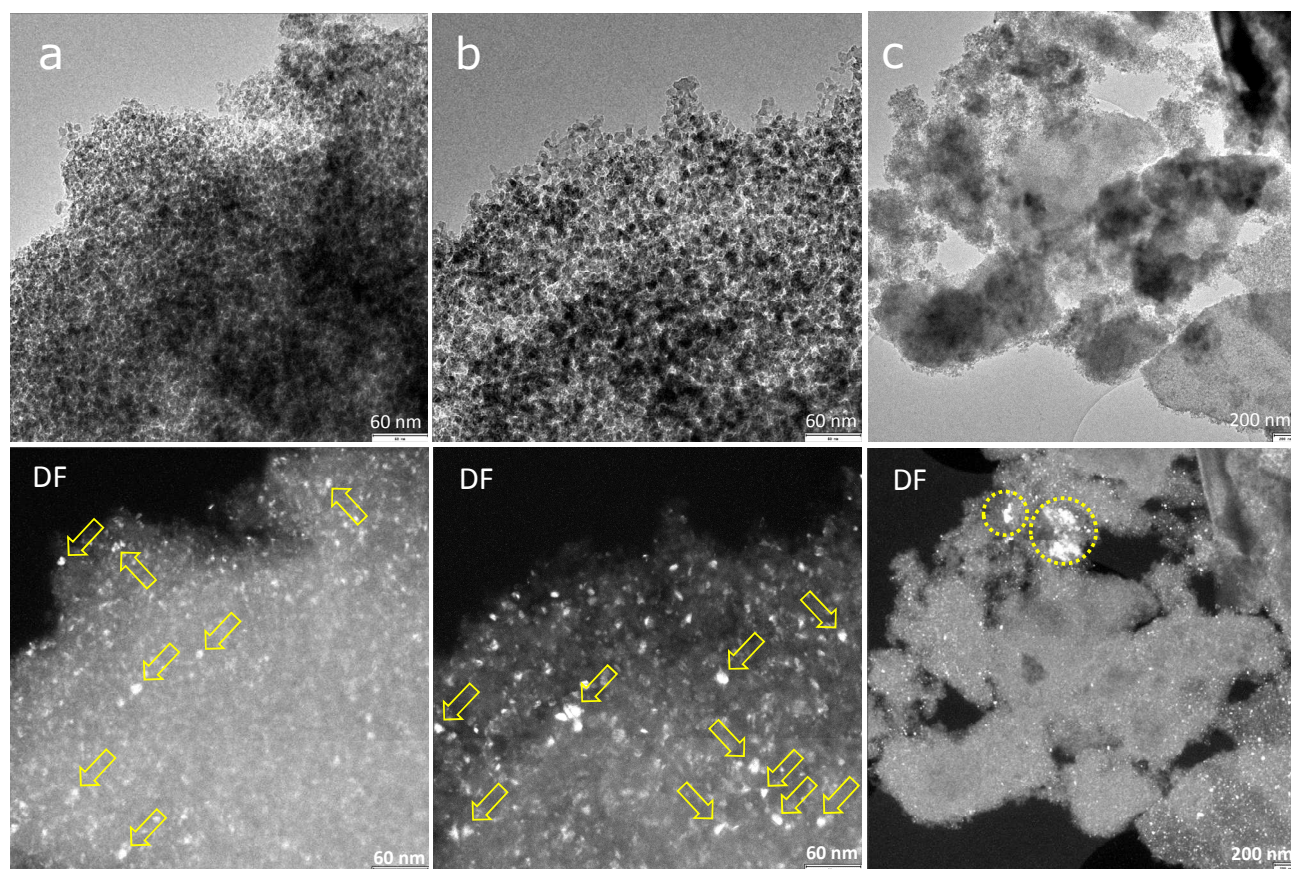
Figure 3. TEM pictures of the TAN-1 material at various magnifications under bright and dark field (DF-TEM, bottom). A high-resolution image can be found in Fig. S-1.

were taken on a Philips CM30T transmission electron microscope. The sample was suspended in isopropanol and then deposited on a holey carbon grid until dryness.

Catalyst preparation and catalytic testing

5 A nickel catalyst supported on TAN-1 was prepared by wet impregnation of nickel nitrate ($Ni(NO_3)_2 \cdot 6H_2O$, Sigma–Aldrich) using a double amount of water with respect to the pore volume obtained by N_2 physisorption. The wet slurry was shaken at 500 rpm for 30 min (VWR, digital DVX-2500). The loading was set 10 at 5 *wt*.%. After impregnation, the sample was dried at 120 °C for 24 h and then calcined at 600 °C at a heating rate of 5 °C/min for 3 h. The as-prepared catalyst was denoted as Ni5/TAN-1. For comparison, a nickel catalyst supported on a commercial MSU-X (denoted as Ni5/MSU-X) was prepared by the same impregnation 15 method. The resulting powders were pelletized, crushed and sieved into a 212-425 μm fraction for the catalytic tests. Steam reforming of CH_4 was carried out in a continuous flow fixed-bed reactor at 850 °C under atmospheric pressure. Prior to the catalytic reaction, the catalyst (*ca.* 100 mg) was reduced with a 20 flow of pure H_2 (16 ml/min NTP) at 850 °C for 1 h. The total feed rate with respect to catalyst weight was 14280 ml/h·g NTP, with a feed composition of $CH_4:H_2O:N_2=1:2:0.3$. The reaction products were periodically analyzed using an on-line gas chromatograph (Varian 450-GC) equipped with a thermal 25 conductivity (TCD) and flame ionization (FID) detectors.

Results

Structural and textural properties of the transitional alumina

The TBAOH mesophase was thermally crystallized under pyrolysis conditions at 1200 °C for various durations. The so-30 obtained materials were characterized by XRD and the patterns are compiled in Figure 2; the crystalline phases detected are summarized in Table l. It was found that when subjecting the mesophase at l h pyrolysis time (TAN-l), besides well-crystallized α-alumina, a transition alumina formed by broad 35 reflections was observed. At the temperature applied α–alumina, with some residues of θ depending on the crystallization time and heating rate,[2,52-55] are the expected phases.

The amplification of the XRD pattern for TAN-l is given in Figure 2, top. Taking into account the high temperature applied, a 40 θ phase[57] would be expected as it is the typical thermal precursor for α-alumina in the (pseudo)boehmite route.[2,52-55] However, a closer look at the pattern evidences that the phase appears to be delta (δ) because of some specific features. Three characteristic reflections between 60 and 65° for θ are missing. The crys-45 tallographic changes from δ to θ are thoroughly described by Rane *et al.;*[59] where the reflection at *ca.* 45.6° typically drops at expense of the one at 32.7° that becomes sharper when the θ phase is formed. These three aspects are missing for the TAN-1 material. Nevertheless, if only δ alumina is present, the reflection 50 at 32.7° should be relatively less intense compared to that at
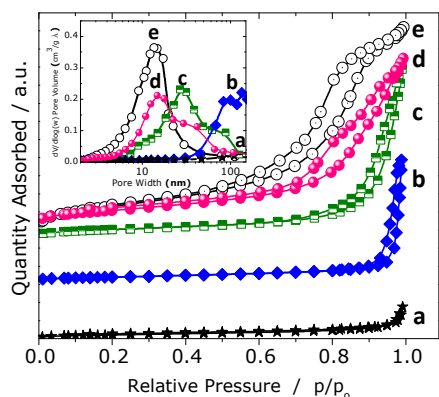
Figure 4. Nitrogen sorption isotherms at -196 °C and corresponding BJH pore size distribution deduced from the adsorption branches (inset): **a)** COM; **b)** TAN-3*a*; **c)** TAN-2; **d)** TAN-4 and **e)** TAN-l. Samples codes are given in Table 1. The isotherms are offset in Y-axis.

45.6°.[60] Based on that, it seems that dispersed θ nuclei can be present as well. We propose that the TAN-1 material is formed by a complex mixture of well-dispersed δ and crystalline α-alumina, and possibly well dispersed θ.

5　　Due to the broad reflections, it is expected that TAN-1 will exhibit a moderately high surface area.

　　When the pyrolysis temperature was increased to 8 h (TAN-2) the material is formed by well-crystallized α and a residue of θ (Fig. 2, and b).

10　　Figure 3 (top) shows the TEM pictures of various TAN-l agglomerates. The texture is formed by a random packing of nanoparticles (Fig. 3-a, -b, top and Fig. S-1) that are highly connected. Using DF-TEM, more crystalline particles can be distinguished, seen as bright spots (arrows in Fig. 3-a, b, bottom),

15 mostly of *ca.* 15-25 nm, that we assign to θ or α alumina domains[52-55] due to the higher bulk density ($3.56 \cdot 10^3$ and $3.98 \cdot 10^3$ kg.m^{-3} for θ and α) compared to δ-alumina ($3.20 \cdot 10^3$ kg.m^{-3}).[50] When an overview picture of an agglomerate is considered (Fig. 3-c, top and bottom), the DF-TEM shows very crystalline

20 domains ranging 100-300 nm (indicated as circles) attributed to α-alumina due to the high crystallinity of this phase shown by the narrow XRD reflections (Fig. 2-top, pattern a). Smaller crystalline domains (around 50-100 nm) are also seen in the overview picture that are ascribed to α phase; θ seems to be

25 unfeasible because the θ to α phase transformation[52-55] takes place via a critical size of around 20 nm for the θ nuclei.

　　Therefore, the TEM is consistent with the previous XRD interpretation; TAN-l is formed by a complex mixture of nanosized δ and more crystalline α-alumina, and possibly θ.

30　　Application of a similar thermal protocol to the TBAOH-free mesophase gives rise to a material composed by pure α-alumina (TAN-3*a*; Fig. 2 pattern c). A similar phase was found when starting with a commercial alumina (COM, pattern d). This contrasts remarkably with TAN-l and points out that the

35 condensation with TBAOH makes the material more resistant to the thermal sintering/coarsening. Furthermore, when the thermal treatment of the TBAOH mesophase is carried out in air, instead of Ar, a mixture of more crystalline α/θ aluminas is formed (TAN-4, Fig. S-2) with lower surface area as will be discussed

40 later. Hence the combined effects of the TBAOH-condensation and the pyrolysis crystallization are essential to retain the nanosized transitional alumina phases.

　　The textural properties of the calcined materials were charac-terized by N_2 physisorption. The adsorption-desorption isotherms

45 and corresponding pore size distributions are shown in Figure 4. The specific BET surface area, pore volume and maxima of the PSD are compiled in Table l. The shape of the isotherms for the thermally treated commercial (COM), TAN-2 and TAN-3*a* is of type IV with hysteresis H3;[61,62] that is found for solids composed

50 of aggregates or agglomerates of particles forming slit-shaped pores. This is consistent with the presence of crystalline large α-alumina particles mainly, as found by XRD. The specific surface area (and pore volume) are relatively low with 7.5 and 10 m^2.g^{-1} for COM and TAN-3*a* because they are composed by well-

55 crystallized α-alumina. When the transition θ alumina is present, TAN-2, the surface area is significantly higher with 23 m^2.g^{-1}. The highest surface area was found for TAN-1 with 64 m^2.g^{-1} and 0.176 cm^3.g^{-1} due to the high content of dispersed transitional aluminas. The shape of the isotherm is different, showing the

60 typical adsorption-desorption of a truly mesoporous material, type IV with hysteresis H1;[61,62] representing solids with cylindrical pore geometry with relatively high pore size uniformity and facile pore connectivity. This is also manifested by the relatively narrow pore size distribution (PSD) centred at

65 13.6 nm as compared to the much wider PSD for the α-alumina-rich materials (Figure 4, inset). The average particle size of the TAN-1 was calculated assuming the particles to be spherical using the S_{BET} and the density for pure δ-alumina ($3.20 \cdot 10^3$ kg.m^{-3}).[50] The particle size was found to be around 30 nm that is

70 consistent with the visualization by TEM (Fig. S-1), notwith-standing that the crystallites have a high degree of aggregation. This comparison proves that the transitional alumina is the major phase present in TAN-1.

　　The directly air-calcined material (TAN-4) has an isotherm

75 type IV, hysteresis H1 with 39 m^2.g^{-1} and a bimodal PSD. The lower specific surface area is in agreement with the presence of more crystalline θ and α phases (Fig. S-2) that contribute less to the surface area.

　　The reproducibility of the TAN-l preparation was verified by

80 comparing the XRD patterns and S_{BET} values for three different batches (Fig. S-3). In all cases, a relatively similar pattern is observed formed by a broad contribution of the transition alumina and narrower α-alumina reflections. There are some fluctuation in the surface area, that is attributed to changes in the relative

85 proportion of the transition phases, as these phases contribute substantially to the surface area.[63,64]

　　The acidic properties of TAN-l were assessed by NH$_3$-TPD in order to quantify the acid types and density. The TPD profile is shown in Figure 5 (left) and compared to a commercial

90 hydrotreatment γ-alumina. The TPD shows two broad desorption peaks centred at *ca.* 250 and 600 °C ascribed to weak and stronger acid sites. The shape of the profile coincides with the commercial hydrotreatment alumina; therefore the acid sites resemble those in a γ-alumina. The specific density of acidic sites

95 by integration of the TPD pattern was found to be 434 given as *a.u./g* (compared to 637 for the hydrotreatment γ-alumina). This value is relatively high and indicates that the surface nature of the TAN-l is relatively acidic.

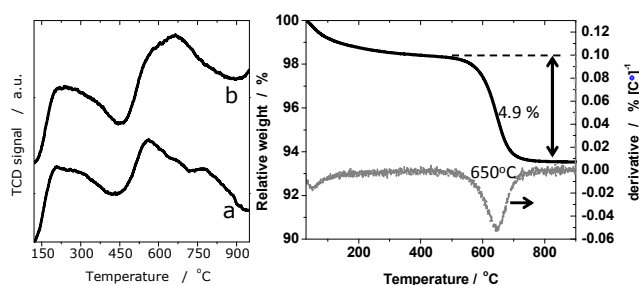The material has a light greyish colour due to a residual carbon,

Figure 5. Left) NH₃-TPD patterns for the TAN-1 material **(a)** compared to the commercial hydrotreatment γ-alumina **(b)**; the patterns are offset in Y-axis. **Right)** TGA pattern in air and derivative for the pyrolyzed TAN-l.

that was found to be of 0.20 *wt.*%. Thus the calcination at 650 °C is not able to fully oxidize the char. This carbon comes from the formation of aluminium (oxy)carbides[65] arising from the reactivity of the char with the alumina during the pyrolysis.

5 **Hydrothermal stability under pure steam and relevant catalytic conditions**

The hydrothermal stability was evaluated by treating the material in a flow of pure steam at 900 °C for 4 and 24 h. XRD patterns for the as-prepared and 24 h-steamed sample are compared in
10 Figure 2, top (patterns **a** and **e**). The reflections of the α-alumina become sharper indicating sintering of this phase into larger particles or transformation of the δ(θ)-phases into more crystalline α; the δ(θ) phases were characterized by broad reflections. The samples were also analysed by gas adsorption
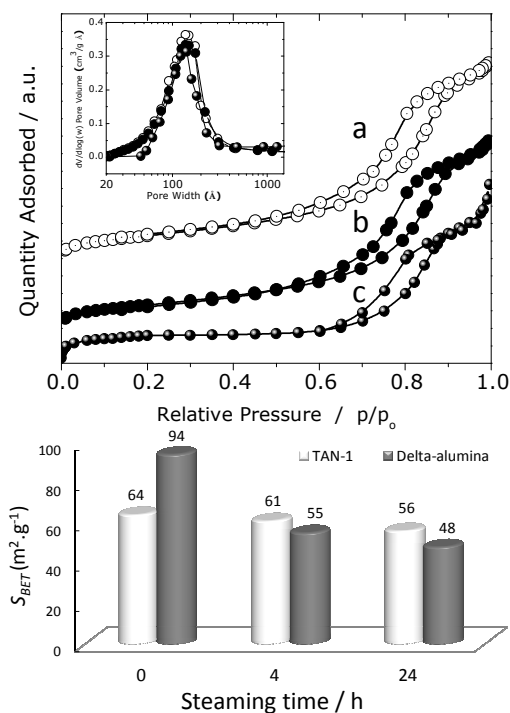15 (Fig. 6). The steamed samples show almost identical isotherm

Figure 6. Stability under steaming (100 *vol.*%, 900 °C) for TAN-l. **Top)** N₂ physisorption isotherms at −196 °C and BJH pore size distributions (inset): **a)** as-prepared material, **b)** after steaming 4 h and **c)** 24 h. The isotherms are offset in Y-axis. **Bottom)** Representation of the S_{BET} as a function of the steaming time for TAN-1 and a pure δ-alumina. Raw data are in Table S-l.
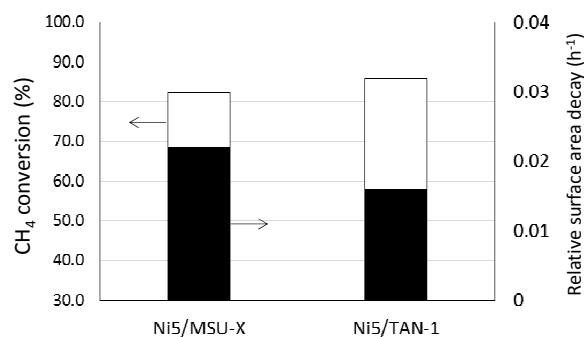

Figure 7. CH₄ conversion (%) after 24 h time on stream and relative surface area decay (h⁻¹) between the fresh and spent catalyst.

shape (type IV-H1) and pore size distributions characteristic of a mesoporous material coming from the δ(θ) nanoparticles, centred at the same position as the fresh TAN-1. Comparison of the specific surface area shows a limited reduction (Table S-1, values
20 are plotted in Fig. 6-bottom); a drop was found from 64 to 61 m².g⁻¹ in 4 h; this represents a surface area rate loss of 0.8 m².g⁻¹.h⁻¹ in the first 4 h, which drops to 0.3 m².g⁻¹.h⁻¹ in the period 4-24 h. Reported deactivation data for pure γ-aluminas lie within 2-20 m².g⁻¹.h⁻¹ and stabilized aluminas (*e.g.* Si-, Ba-, La-based) are
25 between 0.1-3 m².g⁻¹.h⁻¹.[33] This comparison points out that the hydrothermal stability of the TAN-1 appears to be comparable to the additive-stabilized γ-aluminas.

To highlight the impact of the results further, a comparison was done with relevant reference materials, in particular δ-alumina
30 and MSU-X, which were subjected to similar steaming conditions. A pure δ-alumina was prepared according to S. Rane *et al.*[59] The results are compared in Figure 6-bottom (raw data are given in Table S-l). It was found that the initial surface area of the δ-alumina is higher than TAN-l; it however drops severely under
35 steam, with an initial surface area loss of 9.8 m².g⁻¹.h⁻¹ in the 4 h that is almost 12 times higher than TAN-l. The surface area loss in the period 4-24 h was 0.4 m².g⁻¹.h⁻¹ that is 33% higher than TAN-l. The surface area at the end of the tests is lower than the TAN-l. Furthermore, a state-of-the-art γ-alumina (MSU-X) was
40 subjected to similar hydrothermal conditions and compared with TAN-1 as well. The results shown in Fig. S-4 indicate a surface area rate loss of 51 m².g⁻¹.h⁻¹ in the first 4 h, and 2 m².g⁻¹.h⁻¹ between 4 and 24 h, that are 64 and 7 times higher than TAN-1.

The stability was also evaluated as the decay of surface area
45 relative to the initial surface area. The relative decay in the period 0-24 h was found to be 6.7×10⁻³ h⁻¹ (TAN-1), 0.020 h⁻¹ (δ-Al₂O₃) and 0.029 h⁻¹ (MSU-X), which means that δ-Al₂O₃ deactivates under steam nearly 3 times faster and MSU-X 4.3 times faster than TAN-1.

50 The hydrothermal stability of TAN-1 was also investigated under relevant conditions; the steam reforming of CH₄ (SRM) was measured and compared to MSU-X. For this, Ni was incorporated by impregnation and the final activated catalyst was tested in the SRM at 850°C for 24 h time on stream (TOS). After
55 24 h TOS, the Ni5/TAN-1 catalyst shows 3.3 % higher CH₄ conversion than the reference Ni5/MSU-X catalyst (Fig. 7); on average the conversion was *ca.* 2% higher (Fig. S-5). The spent Ni5/TAN-1 catalyst also revealed a lower relative decay of the surface area (40% lower) than the reference catalyst (Fig. 7).
60 These results are consistent with the steam-based hydrothermal

tests and confirm the potential of this novel TAN-1 alumina support, which was prepared without additives.

Formation pathway

The TAN-1 mesophase is formed by an amorphous alumina precursor containing around 90 *wt.*% of organic template that is combusted in air between 200-400 $^{\circ}$C.[46] The TEM and SAXS pattern of the mesophase calcined at 400 $^{\circ}$C show a wormhole structure indicating that the block copolymer was embedded within the alumina precursor before calcination, similarly to the TBAOH-free mesophase.[25,46] Figure 5 (right) shows the typical air-TGA pattern of the pyrolyzed TAN-l indicating that it has 4.9 *wt.*% of char that is decomposed at relatively high temperature, between 550-700 $^{\circ}$C. The formation of char by pyrolysis of a block copolymer $EO_{20}PO_{70}EO_{20}$ requires the presence of surface acidity that catalyses cyclation and aromatization reactions. Such acidity is available on the TAN-1 as shown by the TPD pattern (Fig. 5 left) and it becomes available during the thermal transformation of the amorphous mesophase into the crystalline phases.

Based on the above, a formation scheme for TAN-1 is proposed in Figure 8. The starting mesophase is an amorphous alumina composed by a random distribution of nanoparticles embedded into the block copolymer (Fig. 7, left). After pyrolysis at 1200 $^{\circ}$C for 1 h, the block copolymer is transformed into a cross-linked char structure that is in contact with the crystalized alumina particles (Figure 8, middle). The crystallites that are surrounded by carbon are protected, do not sinter/coarse much and are formed by a well-dispersed δ phase (and possibly θ to less extent). The aggregates that are deficient in char do sinter more and are transformed into the highly crystalline α phase, showing sharp XRD reflections. This step is illustrated in Figure 8, middle. The transformation of the carbon-deficient particles into crystalline α-alumina is explained with a control experiment, TAN-4; this mesophase was treated in air and therefore no protective carbon is present because the template burns between 200-400 $^{\circ}$C.[46] Very crystalline α/θ phases were detected with 39 $m^2.g^{-1}$ that is 40% lower surface area than TAN-1. In this context, some examples where the retention of the organic groups was key to induce (hydro)thermal stability can be cited. The preservation of the organic surfactant during the hydrothermal ageing, was important to induce a high hydrothermal stability for silicas.[66] Porous films of polymer-stabilized Al_2O_3 nanoparticles have been recently reported according to the breath figure technique, having thermal and chemical stability,[67] that resembles to our approach.

In our protocol, the most important effect is nevertheless the TBAOH condensation. When the mesophase is not stabilized (TAN-3*a*), pure α-alumina was obtained with 10 $m^2.g^{-1}$ that is

80% lower surface area than TAN-1. Hence, the stabilization method presented in this study is two-fold; the TBAOH-based condensation produces the largest impact on the surface area and the pyrolysis enables a protective carbon during the crystallization that enhances additionally the surface area. Both make the mesophase more resistant to coarsening/sintering.

Conclusions

A transitional alumina having high steam-based hydrothermal stability has been prepared in three steps: 1) sol-gel hydrolysis of Al-tri-*sec*-butoxide in the presence of $EO_{20}PO_{70}EO_{20}$ where the condensation step is carried out by treating the gel with tetrabutyl ammonium hydroxide; 2) pyrolysis at 1200 $^{\circ}$C for 1 h that produces a char embedding the crystallites and 3) calcination to remove the carbon.

The material is formed by a complex mixture of δ, α and possibly θ aluminas; it has well-defined mesopores with surface areas ranging 59-76 $m^2.g^{-1}$ that can withstand steam conditions at 900 $^{\circ}$C with low surface area rate loss. The hydrothermal stability is also confirmed after adding Ni under relevant methane steam reforming conditions; a decreased surface area decay and superior performance than a state-of-the art MSU-X support was found.

The key aspects to obtain such material are the TBAOH condensation that makes the final material more stable against thermal sintering, reducing the formation of crystalline θ/α aluminas; secondly, in minor proportion, the protective effect of the char formed during the pyrolysis, which embeds the crystallites and reduces the thermal sintering as well.

References

1. F. Schüth, S.W.S. Kenneth, and J. Weitkamp (Eds.), *Handbook of Porous Solids*, Wiley-VCH; Weinheim, 2002, p. 1605.
2. J. R. Regalbuto and G.J. Antos in G.J. Antos, A.M. Aitani (Eds.), *Catalytic Naphtha Reforming: Science and Technology*, 2nd Ed., Marcel Dekker, Inc., 2004, Chapter 5, p. 144.
3. J. R. Regalbuto and G.J. Antos in G.J. Antos, A.M. Aitani (Eds.), *Catalytic Naphtha Reforming: Science and Technology*, 2nd Ed., Marcel Dekker, Inc., 2004, Part II. Reforming catalysts.
4. H. Topsoe, B.S. Clausen, F.E. Massoth, "*Hydrotreating Catalysis, Science and Technology*", Springer, Berlin, **1996**.
5. C. Márquez-Alvarez, N. Zilkova, J. Perez-Pariente, J. Cejka, *Catal. Rev. Sci. Eng.* 2008, **50**, 222.
6. M. Yada, H. Kitamura, M. Machida, T. Kijima, *Langmuir* 1997, **13**, 5252.
7. M. Yada, H. Hiyoshi, K. Ohe, M. Machida, T. Kijima, *Inorg. Chem.*, 1997, **36**, 5565.
8. M. Yada, M. Ohya, M. Machida, T. Kijima, *Chem. Commun.*1998, 1941.
9. V. González-Peña, I. Díaz, C. Márquez-Álvarez, E. Sastre, J. Pérez-Pariente, *Micropor. Mesopor. Mat.* 2001, **44**, 203.
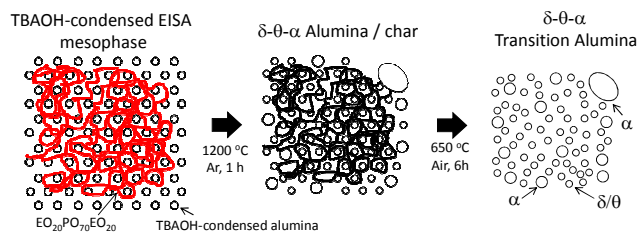10. H.Y. Zhu; J.D. Riches, J.C. Barry, *Chem. Mater.* 2002, 14, 2086.

Figure 8. Proposed mechanism for the formation of the transition alumina (TAN-l) that is stabilized by *in-situ* char generation under pyrolysis conditions followed by calcination of a TBAOH condensed Al-mesophase. Particle aggregation occurs in practice; it is omitted in this scheme for simplicity.

11. Z. Zhang, R.W. Hicks, T. Pauly, T.J. Pinnavaia, *J. Am. Chem. Soc.* 2002, **124**, 1592.
12. Z. Zhang, T.J. Pinnavaia, *J. Am. Chem. Soc.* 2002, **124**, 12294.
13. R.W. Hicks, T.J. Pinnavaia, *Chem. Mater.* 2003, **15**, 78.
14. H.C. Lee, H.J. Kim, S.H. Chung, K.H. Lee, H.C. Lee, J.S. Lee, *J. Am. Chem. Soc.* 2003, **125**, 2882.
15. M. Kuemmel, D. Grosso, C. Boissiere, B. Smarsly, T. Brezesinski, P.A. Albouy, H. Amenitsch, C. Sanchez, *Angew. Chem., Int. Ed.* 2005, **44**, 4589.
16. C. Boissiere, L. Nicole, C. Gervais, F. Babonneau, M. Antonietti, H. Amenitsch, C. Sanchez, D. Grosso, *Chem. Mater.* 2006, **18**, 5238.
17. Q. Liu, A.Q. Wang, X.D. Wang, T. Zhang, *Chem. Mater.* 2006, **18**, 5153.
18. Z.X. Wu, Q. Li, D. Feng, P.A. Webley, D.Y. Zhao, *J. Am. Chem. Soc.* 2010, **132**, 12042.
19. H. Park, S.H. Yang, Y.S. Jun, W.H. Hong, J.K. Kang, *Chem. Mater.* 2007, **19**, 535.
20. Q. Yuan, A.X. Yin, C. Luo, L.D. Sun, Y.W. Zhang, W.T. Duan, H.C. Liu, C.H. Yan, *J. Am. Chem. Soc.* 2008, **130**, 3465.
21. S.M. Morris, P.F. Fulvio, M. Jaroniec, *J. Am. Chem. Soc.* 2008, **130**, 15210.
22. Z. Zhang, T.J. Pinnavaia, *Langmuir* 2010, **26**, 10063.
23. Q.L. Wu, F. Zhang, J.P. Yang, Q. Li, B. Tu, D.Y. Zhao, *Micropor. Mesopor. Mat.* 2011, **143**, 406.
24. L.L. Li, W.T. Duan, Q. Yuan, Z.X. Li, H.H. Duan, C.H. Yan, *Chem. Commun.* 2009, 6174.
25. L. López Pérez, S. Perdriau, G. ten Brink, B.J. Kooi, H.J. Heeres, I. Melián-Cabrera, *Chem. Mater.* 2013, **25**, 848
26. C.H. Bartholomew, R.J. Farrauto, *Fundamentals of Industrial Catalytic Processes*, Second Edition, John Wiley & Sons, Inc., 2006, p. 716.
27. M. Machida, K Eguchi, H. Arai, *J. Catal.* 1989, **120**, 377.
28. G. Groppi, M. Bellotto, C. Cristiani, P. Forzatti, P.L. Villa, *Appl. Catal. A: Gen.* 1993, **104**, 101.
29. H. Arai, M. Machida, *Appl. Catal. A: Gen.* 1996, **138**, 161.
30. H. Arai, T. Yamada, K. Eguchi, T. Seiyama, *Appl. Catal.* 1986, **26**, 265.
31. S. Ponce, M.A. Peña, J.L.G. Fierro, *Appl. Catal. B: Environ.* 2000, **24**, 193.
32. B.E. Yoldas, *J. Mater. Sci.* 1976, **11**, 465.
33. M.F.L. Johnson, *J. Catal.* 1990, **123**, 245.
34. B. Béguin, E. Garbowski, M. Primet, *J. Catal.* 1991, **127**, 595.
35. J.B. Miller, E.I. Ko, *Catal. Today* 1998, **43**, 51.
36. T. Horiuchi, L. Chen, T. Osaki, T. Sugiyama, K. Suzuki, T. Mori, *Catal. Lett.* 1999, **58**, 89.
37. W. Daniel, U. Schubert, R. Glöckler, A. Meyer, K. Noweck, H. Knözinger, *Appl. Catal. A: General* 2000, **196**, 247.
38. T. Horiuchi, T. Osaki, T. Sugiyama, K. Suzuki, T. Mori, *J. Non-Cryst. Solids* 2001, **291**, 187.
39. T. Osaki, K. Nagashima, K. Watari, K. Tajiri, *J. Non-Cryst. Solids* 2007, **353**, 2436.
40. O. Mekasuwandumrong, P. Tantichuwet, C. Chaisuk, P. Praserthdam, *Mat. Chem. Phys.* 2008, **107**, 208.
41. K. Kosuge, A. Ogata, *Micropor. Mesopor. Mater.* 2010, **135**, 60.
42. B. Béguin, E. Garbowski, M. Primet, *Appl. Catal.* 1991, **75**, 119.
43. J.S. Church, N.W. Cant, D.L. Trimm, *Appl. Catal. A: Gen.* 1993, **101**, 105.
44. M. Machida, K Eguchi, H. Arai, *J. Catal.* 1987, **103**, 385.
45. P. Burtin, J.P. Brunelle, M. Pijolat, M. Soustelle, *Appl. Catal.*, 1987, **34**, 225.
46. L. López Pérez, V. Zarubima, H.J. Heeres, I. Melián-Cabrera, *Chem. Mater.* **DOI:** 10.1021/cm401443b.
47. S. Brunauer, P.H. Emmett, E. Teller, *J. Am. Chem. Soc.* 1938, **60**, 309.
48. E.P. Barrett, L.G. Joyner, P.H. Halenda, *J. Am. Chem. Soc.* 1951, **73**, 373.
49. B.C. Lippens, J.H. de Boer, *J. Catal.* 1965, **4**, 319.
50. G. MacZura, "Aluminum Oxide (Alumina), Calcined, Tabular, and Aluminate Cements", in *Kirk-Othmer: Encyclopedia of Chemical Technology*; published online on 17 Jan 2003, DOI: 10.1002/0471238961. 0301120313010326.a01.pub2, 2001 by John Wiley & Sons, Inc. Vol. 2 p. 406.

51. M.J. Ortiz-Iniesta, H.J. Heeres, I. Melián-Cabrera, *Micropor. Mesopor. Mat.* 2013, **171**, 208.
52. H.L. Wen, Y.Y. Chen, F.S. Yen, C.Y. Huang, *Nanostruct. Mater.* 1999, **11**, 89.
53. H.L. Wen, F.S. Yen, *J. Cryst. Growth* 2000, **208**, 696.
54. F.S. Yen, H.L. Wen, Y.T. Hsu, *J. Cryst. Growth* 2001, **233**, 761.
55. P.L. Chang, F.S. Yen, K.C. Cheng, H.L. Wen, *Nano Lett.* 2001, **1**, 253.
56. JCPDS file no: 10-173.
57. R.S. Zhou, R.L. Snyder, *Acta. Crystallogr. Sect. B: Struct. Sci.* 1991, **47**, 617.
58. JCPDS file no: 4-877.
59. S. Rane, Ø. Borg, J. Yang, E. Rytter, A. Holmen, *Appl. Catal. A: Gen.* 2010, **388**, 160.
60. T.J. Webster, E.L. Hellenmeyer, R.L. Price, *Biomaterials* 2005, **26**, 953.
61. K.S.W. Sing, D.H. Everett, R.A.W. Haul, L. Moscou, R. Pierotti, J. Rouquerol, T. Siemieniewska, *Pure Appl. Chem.* 1985, **57**, 603.
62. M. Kruk, M. Jaroniec, *Chem. Mater.* 2001, **13**, 3169.
63. X. Zhang, Y. Ge, S.-P. Hannula, E. Levänen, T. Mäntylä, *J. Mater. Chem.* 2008, **18**, 2423.
64. X. Zhang, Y. Ge, S.-P. Hannula, E. Levänen, T. Mäntylä, *J. Mater. Chem.* 2009, **19**, 1915.
65. J.M. Lihrmann, T. Zambetakis, M. Daire, *J. Am. Ceram. Soc.* 1989, **72**, 1704.
66. D. Pan, P. Yuan, L. Zhao, N. Liu, L. Zhou, G. Wei, J. Zhang, Y. Ling, Y. Fan, B. Wei, H. Liu, C.Z. Yu, X. Bao, *Chem. Mater.* 2009, **21**, 5413.
67. Y. Saito, M. Shimomura, H. Yabu, *Chem. Commun.* 2013, **49**, 6081.

Graphical abstract

TBAOH-condensed EISA mesophase → (PYROLYSIS, 1200 °C, Ar, 1 h) → δ-θ-α Alumina / char → (CALCINATION, 650 °C, Air, 6h) → δ-θ-α Transition Alumina

$EO_{20}PO_{70}EO_{20}$ Alumina precursor

α δ/θ

HYDROTHERMALLY STABLE